A&A 679, L11 (2023)
https://doi.org/10.1051/0004-6361/202348126

Astronomy & Astrophysics

LETTER TO THE EDITOR

An infrared FWHM–K_2 correlation to uncover highly reddened quiescent black holes

V. A. Cúneo[1,2], J. Casares[1,2], M. Armas Padilla[1,2], J. Sánchez-Sierras[1,2], J. M. Corral-Santana[3,4], T. J. Maccarone[5], D. Mata Sánchez[1,2], T. Muñoz-Darias[1,2], M. A. P. Torres[1,2], and F. Vincentelli[1,2]

[1] Instituto de Astrofísica de Canarias (IAC), Vía Láctea s/n, 38205 La Laguna, Tenerife, Spain
e-mail: virginiacuneo@gmail.com
[2] Departamento de Astrofísica, Universidad de La Laguna, Av. Astrofísico Francisco Sánchez s/n, 38206 La Laguna, Tenerife, Spain
[3] European Southern Observatory (ESO), Alonso de Córdova 3107, Vitacura, Casilla 19, Santiago, Chile
[4] Pontificia Universidad Católica de Chile, Vicuña-Mackenna 4860, Macul, Santiago, Chile
[5] Department of Physics & Astronomy, Texas Tech University, Box 41051, Lubbock, TX 79409-1051, USA

Received 2 October 2023 / Accepted 26 October 2023

ABSTRACT

Among the sample of Galactic transient X-ray binaries (SXTs) discovered to date, about 70 have been proposed as likely candidates to host a black hole. Yet, only 19 have been dynamically confirmed. Such a reliable confirmation requires phase-resolved spectroscopy of their companion stars, which is generally feasible when the system is in a quiescent state. However, since most of the SXT population lies in the galactic plane, which is strongly affected by interstellar extinction, their optical brightness during quiescence usually falls beyond the capabilities of the current instrumentation ($R \gtrsim 22$). To overcome these limitations and thereby increase the number of confirmed Galactic black holes, a correlation between the full-width at half maximum (FWHM) of the Hα line and the semi-amplitude of the donor's radial velocity curve (K_2) was presented in the past. Here, we extend the FWHM–K_2 correlation to the near-infrared (NIR), exploiting disc lines such as He I λ10830, Paγ, and Brγ, in a sample of dynamically confirmed black-hole SXTs. We obtain $K_2 = 0.22(3)$ FWHM, in good agreement with the optical correlation derived using Hα. The similarity of the two correlations seems to imply that the widths of Hα and the NIR lines are consistent in quiescence. When combined with information on orbital periods, the NIR correlation allows us to constrain the mass of the compact object of systems in quiescence by using single-epoch spectroscopy. We anticipate that this new correlation will give access to highly reddened black hole SXTs, which cannot be otherwise studied at optical wavelengths.

Key words. accretion, accretion disks – black hole physics – stars: black holes – stars: neutron

1. Introduction

Black holes (BHs) have long been subject of intense study due to their display of extreme physics, such as accretion and outflows, which is common to sources at all scales, from X-ray binaries to active galactic nuclei (e.g., Fabian 2012; Fender & Muñoz-Darias 2016). In particular, stellar-mass BHs provide the ideal laboratories to study the phenomenon of accretion on timescales suitable for human investigation. In addition, BHs with known masses play a key role in testing and understanding the supernova explosion mechanism and the formation of compact objects (e.g., Belczynski et al. 2012; Casares et al. 2017).

Four techniques are currently used to find stellar-mass BHs, with each offering some advantages and some limitations relative to the others. Gravitational waves have now detected large samples of BHs (e.g., Abbott et al. 2023), but are strongly biased toward the more massive objects. Orbital measurements of the companion stars in detached BH binaries (e.g., Giesers et al. 2018; El-Badry et al. 2023) and microlensing detections (e.g., Lam et al. 2022; Sahu et al. 2022) enable the detection of BHs without strong interactions with their environment, but offer no probes of the BH spins. Transient X-ray binaries (so called soft X-ray transients, SXTs) offer the opportunity to use X-rays to probe spins (e.g., Reynolds 2021), but they typically form via common envelope evolution and, hence, may not be representative of the global mass distribution. Generally, SXTs are discovered when they enter a usually short-lived but bright outburst phase (see Corral-Santana et al. 2016 for a review; see also McClintock & Remillard 2006). They host either a neutron star (NS) or a BH that accretes matter from a low-mass ($\leq 1\,M_{\odot}$) donor star through an accretion disc.

To date, ~70 BH candidates have been detected in SXTs (e.g., Corral-Santana et al. 2016; Tetarenko et al. 2016). However, an empirical extrapolation of that sample implies that about 2000 BH SXTs are expected to exist in the Galaxy (Romani 1998; Corral-Santana et al. 2016), while some population-synthesis models predict that the number ought to be $\geq 10^4$ (Kiel & Hurley 2006; Yungelson et al. 2006). In addition to the low detection statistics, determining the BH nature of the compact object in these systems represents a problem in itself. We need to estimate the mass of the compact component in order to confirm its nature, which requires phase-resolved spectroscopy to perform optical dynamical studies of the low-mass companion star (e.g., Casares et al. 1992; Torres et al. 2019). Given that during outburst the accretion disc is so bright that it conceals

Table 1. Sample of SXTs used in this work.

X-ray transient	Type	Spectra	Observing period	Resolution (km s^{-1})	Spectral band	Telescope/ instrument	References
Nova Mus 1991	BH	17 × 1200 s	13/04/13–10/05/13	70	J, H, K	VLT/X-shooter	1
A0620-00	BH	12 × 240 s	17/02/05	150	K	Keck II/NIRSPEC	2
XTE J1118+480	BH	48 × 310 s	02/04/11 and 12/04/11	176	J, H, K	Gemini/GNIRS	3
GX 339-4	BH	16 × 275 s	22/05/16–07/09/16	55	J, H	VLT/X-shooter	4
GRS 1915+105	BH	27 × 2400 s	09/06/10–03/09/11	37	J, H, K	VLT/X-shooter	5
Aql X-1	NS	24 × 900 s	20/05/10–29/09/11	75	K	VLT/SINFONI	6

References. (1) González Hernández et al. (2017); (2) Harrison et al. (2007); (3) Khargharia et al. (2013); (4) Heida et al. (2017); (5) Steeghs et al. (2013); (6) Mata Sánchez et al. (2017).

entirely the companion star, these studies are done in quiescence, when the optical brightness of the binary is dominated by the donor, with the addition of broad emission lines that evidence the presence of the accretion disc (e.g., Charles & Coe 2006). On the one hand, this represents an advantage, since SXTs spend most of the time in the quiescent state. On the other hand, the companion is a low-mass, and therefore an intrinsically faint, star whose apparent brightness usually falls beyond the observing threshold of the largest available telescopes, namely, $R \gtrsim 22$. We refer to Corral-Santana et al. (2011) and Yanes-Rizo et al. (2022) for examples of dynamical studies of the companion star at the limit of the instrumental capabilities. We are therefore biased towards detecting BHs only in the brightest and closest systems. As a result, from the sample of BH candidates, only 19 have been dynamically confirmed (Casares & Jonker 2014; Corral-Santana et al. 2016; see online version of BlackCAT[1]).

Based on the fact that the emission lines from the quiescent disc, particularly Hα, are much stronger (with larger equivalent widths) than the absorption lines from the companion star, Casares (2015) proposed a novel technique to determine the mass of a BH. This approach can reach systems ~2.5 mag fainter than with the classical dynamical studies. The method, which relies on a scaling correlation between the full width at half-maximum (FWHM) of Hα and the projected velocity semi-amplitude of the companion star (K_2), allows us to uncover new BH SXTs by solely resolving Hα and knowing the orbital period ($P_{\rm orb}$; Mata Sánchez et al. 2015; Casares 2018).

SXTs with quiescent R magnitudes fainter than ~22–24 can either be intrinsically faint or extincted by interstellar material. Most of the detected BH SXT candidates are located along the galactic plane, where interstellar extinction is usually high. The infrared spectral region is significantly less affected by the extinction (e.g., Wang & Chen 2019) and it is therefore appropriate for investigating new techniques to uncover BHs (e.g., Steeghs et al. 2013). In this work, we extend the method from Casares (2015) to the near-infrared (NIR) regime. To this aim, we investigate the typical emission lines present in the NIR spectra of known SXTs. The NIR FWHM–K_2 correlation allows us to measure masses of the compact objects in optically faint SXTs, based on single-epoch spectroscopy datasets.

2. The sample

We compiled a spectroscopy sample of five dynamically confirmed BH SXTs from the BlackCAT catalogue and a NS SXT, exhibiting He I λ10830, Paγ and/or Brγ in emission during the quiescent state. Table 1 contains a summarised observing log for each system, including references to the literature with the original publication for further details. We downloaded and reduced the data for A0620-00 (first published by Harrison et al. 2007) using the WMKONSPEC package and usual IRAF[2] tasks. We used the GEMINI IRAF package to process the XTE J1118+480 spectra, first presented in Khargharia et al. (2013). In addition, we downloaded the Nova Mus 1991, GX 339-4, and GRS 1915+105 data published in González Hernández et al. (2017), Heida et al. (2017), and Steeghs et al. (2013), respectively, and processed them using the ESO X-shooter pipeline v.3.5.0. In the case of Aql X-1, we used the spectra published and reduced in Mata Sánchez et al. (2017).

We acknowledge that since its discovery outburst in 1992, GRS 1915+105 was never in a fully quiescent state. Its X-ray flux was highly variable until 2018, when it decayed to a low-flux plateau (e.g., Motta et al. 2021). Nonetheless, the large size of the accretion disc ($P_{\rm orb} = 33.85 \pm 0.16$ days) and the fact that the donor star is not affected by irradiation (Steeghs et al. 2013), imply that irradiation in the outer disc (where the emission lines that we analyse are formed; see Sect. 3) is modest. In addition, most of the data used in this study were obtained in periods of faint X-ray emission. Therefore, we expect the emission lines included in our analysis to behave like in a quiescent disc.

He I λ10830 and Paγ are in relatively clean spectral regions. However, Brγ is in a spectral region where the atmosphere contribution might be significant, which requires the application of techniques for correction from telluric features. The GRS 1915+105 spectra were corrected from telluric absorptions of H_2O and CH_4 molecules using MOLECFIT v.3.0.3. The use of IRAF tasks together with spectra from a telluric star was undertaken for the correction of A0620-00 spectra, while custom software under PYTHON was used for the case of Aql X-1.

3. The FWHM–K_2 correlation

We focused our analysis on the strongest NIR transitions present in the data (He I λ10830, Paγ and/or Brγ) using MOLLY and custom software under PYTHON 3.7. We carefully normalised each emission line by fitting the adjacent continuum with a low order polynomial and we combined the spectra to obtain one single spectrum per line and source with a higher signal-to-noise ratio (S/N). The FWHM values were obtained from fitting each emission line with a model consisting of a Gaussian profile plus a constant, over a spectral region of ±10 000 km s^{-1} around the line rest wavelength (with the exception of GRS 1915+105, for

[1] BlackCAT: https://www.astro.puc.cl/BlackCAT/

[2] IRAF is distributed by the National Optical Astronomy Observatory, which is operated by the Association of Universities for Research in Astronomy, Inc. under contract to the National Science Foundation.

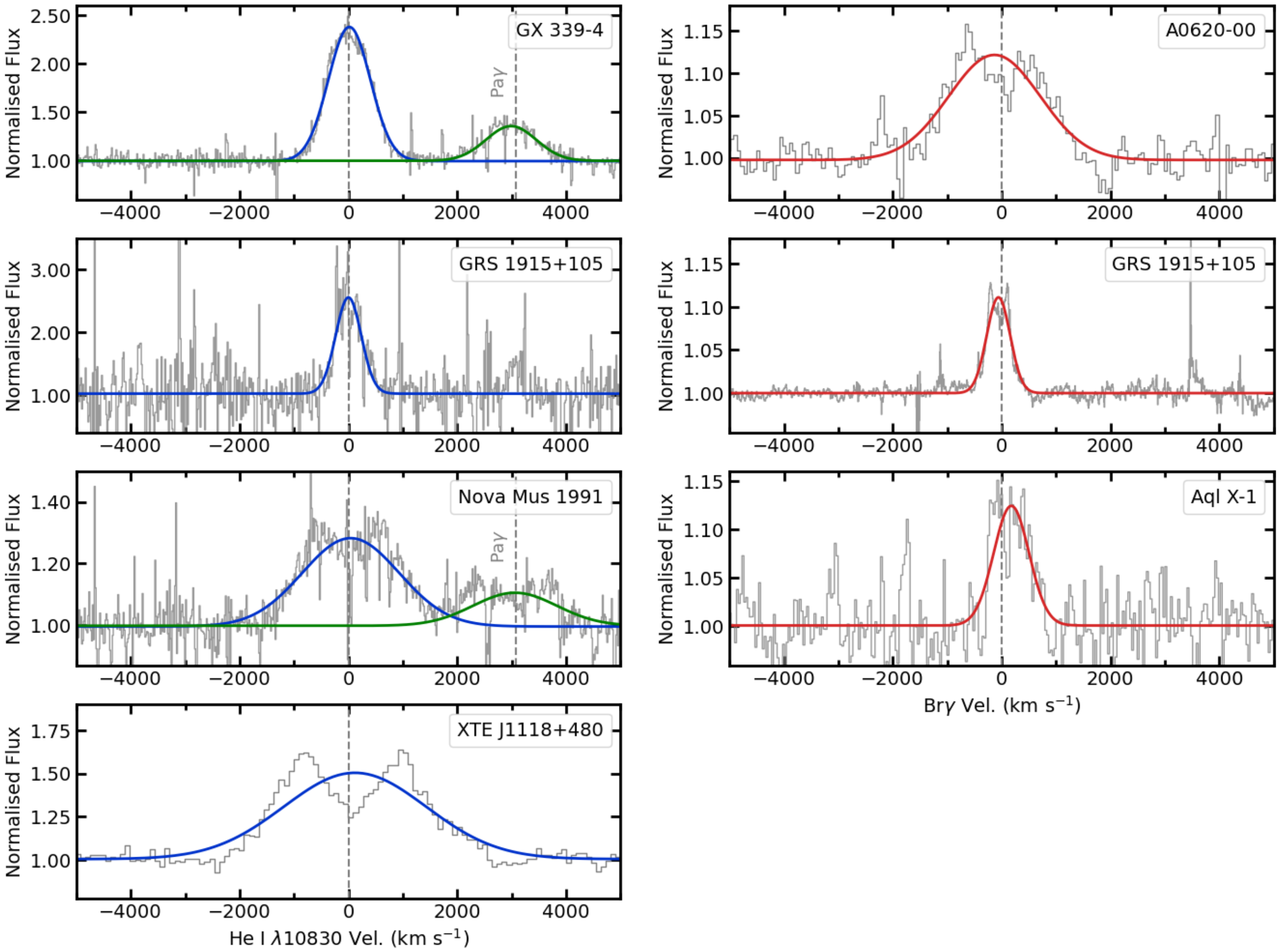

Fig. 1. Gaussian fits to the NIR emission line profiles. The left column shows the fits for the He I λ10830 (blue) and Paγ (green; when the S/N allowed to fit the line) emission lines, while the fits to Brγ (red) are shown in the right column.

which we used a spectral region of $\pm$4000 km s^{-1} to avoid contamination by nearby instrumental features). We used orthogonal distance regression in the ordinary least squares mode, implementing the PYTHON package SCIPY.ODR, to perform these fits. We notice that some of the lines present the double-peaked profile caused by the rotation of the disc (Smak 1969). However, following Casares (2015), we decided to fit a Gaussian to all the data, which is a more robust model than a double-Gaussian. While the double-Gaussian might fail to fit data of limited spectral resolution and poor S/N, Casares (2015) found that the FWHM values obtained from a single-Gaussian are within a 10% of those obtained with more complex models. In the case of He I λ10830, the neighbouring Paγ emission line was masked when present – and vice versa.

Spectral variations from one epoch to another may be present and can be caused by aperiodic flares and orbital changes, such as disc asymmetries (Hynes et al. 2002; Casares 2015). However, in most cases we are limited by the S/N, which can reflect the observing conditions of the night. In order to estimate the impact of additional systematics related to the intrinsic variability of the FWHM we used the spectra of GX 339-4, which exhibit the highest S/N data in our sample. A Gaussian fit allowed us to estimate the FWHM value of the He I λ10830 line, along with its corresponding standard deviation, for each of the 16 spectra individually. We then used both the error propagation and the standard deviation to obtain a more conservative error (of ~10%) for the combined data of GX 339-4. Then, for the remaining sources of the sample we estimated the error of the FWHM as the quadratic sum of the statistical error from the fit and the 10% of the FWHM. To obtain the intrinsic FWHMs, we subtracted the instrumental resolution quadratically. Figure 1 displays the fits to each line included in our sample. In Table 2, we list the FWHM values we measured, as well as the residual variance (σ_r^2), which parameterises the quality of the Gaussian fits by quantifying deviations between the data and the best-fitting model, as well the dynamical K_2 values with their corresponding references. We note that the reported value of σ_r^2 for the fit of the He I λ10830 line in GX 339-4 in Table 2 is an average of the 16 σ_r^2 values from the individual fits.

In the top panel of Fig. 2, we display the FWHM values versus K_2 for the SXTs in our sample. A linear fit, using orthogonal distance regression to account for errors in both FWHM and K_2 values, yields the following relation:

$$K_2 = 0.22(3)\,FWHM, \tag{1}$$

where both K_2 and FWHM are given in km s^{-1}. The residual variance is $\sigma_r^2 = 1.04$. Allowing for a constant term does not

Table 2. SXT parameters.

X-ray transient	Emission line	$FWHM$ (km s^{-1})	σ_r^2	K_2 (km s^{-1})	K_2 from corr. (km s^{-1})	P_{orb} (days)	$f(M)$ ($M_\odot$)	PMF ($M_\odot$)	Ref.
Nova Mus 1991	He I λ10830	2097 ± 213	26.07	406.8 ± 2.7	461 ± 78	0.43260249(9)	3.02 ± 0.06	4.4 ± 2.2	(1)
	Paγ	1811 ± 197	26.06		398 ± 69			2.8 ± 1.5	
A0620-00	Brγ	1974 ± 204	4.31	437.1 ± 2.0	434 ± 74	0.32301405(1)	2.79 ± 0.04	2.7 ± 1.4	(2)
XTE J1118+480	He I λ10830	3078 ± 310	20.06	708.8 ± 1.4	677 ± 115	0.1699338(5)	6.27 ± 0.04	5.5 ± 2.8	(3)
GX 339-4	He I λ10830	900 ± 77	4.18	219.0 ± 3.0	198 ± 32	1.7587(5)	1.91 ± 0.08	1.4 ± 0.7	(4)
	Paγ	1088 ± 111	5.76		239 ± 41			2.5 ± 1.3	
GRS 1915+105	He I λ10830	551 ± 59	6.72	126.0 ± 1.0	121 ± 21	33.85(16)	7.02 ± 0.17	6.2 ± 3.2	(5)
	Brγ	503 ± 50	44.34		111 ± 19			4.8 ± 2.4	
Aql X-1	Brγ	762 ± 86	2.45	136.0 ± 4.0	168 ± 30	0.7895126(10)	0.21 ± 0.02	0.4 ± 0.2	(6)

References. (1) Wu et al. (2015); (2) González Hernández & Casares (2010); (3) González Hernández et al. (2012); (4) Heida et al. (2017); (5) Steeghs et al. (2013); (6) Mata Sánchez et al. (2017).

improve the fit since it is consistent with zero at 1σ. We computed the K_2 values from this relation (see Table 2) and compared them with the dynamical estimations, finding that the differences follow a Gaussian distribution with a standard deviation of 26 km s^{-1}. We estimated the error of the coefficient in Eq. (1) as the quadratic sum of the statistical error from the fit and the result from a Monte Carlo simulation of 10^4 events, imposing the condition that the difference between the model and the real K_2 values follow a Gaussian distribution with σ = 26 km s^{-1}. It is worth mentioning that although GRS 1915+105 was not in full quiescence, and its FWHM values define the bottom end of the correlation, the best-fit parameters remain within the error if we remove those points from the fit.

Casares (2015) derived an analogous relation in the optical (K_2 = 0.233(13) FWHM) using the FWHM of the Hα emission line. We show this data in the bottom panel of Fig. 2. We notice that our NIR correlation (Eq. (1)) is fully compatible with that of Hα. Furthermore, a single fit to the combined Hα and NIR FWHM values yields best-fit parameters that are fully consistent with both the optical and NIR correlations.

As explained in Sect. 3 of Casares (2015), the FWHM–K_2 correlation is expected from basic equations. Particularly, for BH SXTs with a typical mass ratio q = 0.1, $K_2/FWHM = 0.36\sqrt{\alpha}$, where α is the ratio between the disc radius at which the FWHM is determined by gas velocity (R_W) and the effective radius of the compact object's Roche lobe (R_{L1}). Our correlation entails that the FWHM of the NIR emission lines trace the disc velocity at 37% R_{L1}, implying that these lines are formed in the outer regions of the disc (as is the case for Hα).

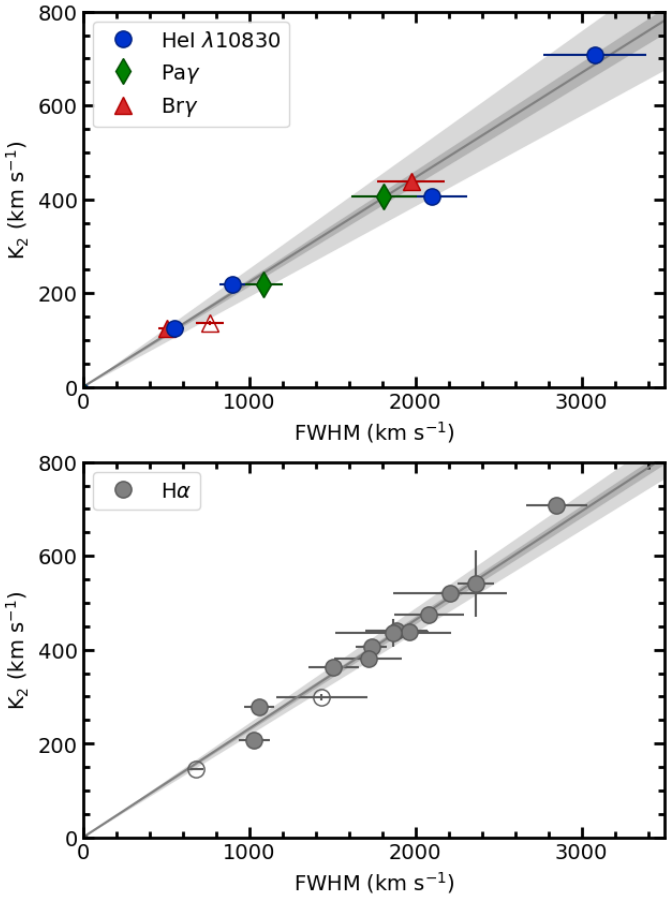

Fig. 2. FWHM–K_2 correlation for SXTs with the best linear fit, using NIR (top panel) and optical (bottom panel; data come from Casares 2015) emission lines. Filled symbols indicate BH binaries, while NS binaries are denoted with open symbols. The shaded regions in both plots correspond to the 1σ uncertainty of the linear fit (dark grey) and the total uncertainty of the correlation that includes the result from the Monte Carlo simulation in Sect. 3 (light grey).

4. Discussion

With the aim of uncovering and studying the reddened population of BHs in the Galaxy, in this work, we compiled the NIR spectra of dynamically studied BH SXTs and a system with a NS during quiescence. We found a correlation between the FWHM of He I λ10830, Paγ, and Brγ emission lines, and K_2 (upper panel in Fig. 2). Despite the low statistics due to the limited availability of NIR spectra of SXTs in quiescence, a comparison with the analogous relation found by Casares (2015) at optical wavelengths, using the Hα emission line (bottom panel of Fig. 2), offers evidence of their resemblance, turning the NIR correlation into a reliable tool. Even the correlation of the combined optical and NIR data agrees with the two separate correlations, as mentioned in Sect. 3.

These correlations allow one to obtain K_2 by measuring the FWHM in quiescence of either Hα or one of the NIR emission lines used in this study. This method only requires one single spectrum with an emission line, which saves considerable observing time when compared to the phase-resolved spectroscopy needed by the classical method (radial velocities) to estimate K_2. We note, however, that a large orbital coverage would be ideal to avoid potential orbital variations. Nonetheless, an error equal to the quadratic sum of 10% of the FWHM and the statistical error (see Sect. 3) can be assumed in the FWHM values when a single spectrum is available.

Most importantly, the FWHM–K_2 correlations are fundamental to uncover the hidden (reddened) population of quiescent BHs in the Galaxy (Jonker et al. 2021). By combining Eq. (1) with $P_{\rm orb}$, we can use Kepler's third law to estimate a preliminary mass function PMF $= 1.1 \times 10^{-9}\, P_{\rm orb}\, FWHM^3$, where PMF is in units of $M_\odot$, $P_{\rm orb}$ in days, and FWHM in km s^{-1} (see Casares 2015 for the optical analogue). The PMF gives a lower limit to the mass of the compact component in the binary system from single epoch spectroscopy. For PMF $\gtrsim 3\, M_\odot$, the assumed approximate mass limit to segregate BHs from NSs (e.g., Kalogera & Baym 1996; Rezzolla et al. 2018), we can positively confirm the BH nature of the compact object. Table 2 includes $P_{\rm orb}$, as well as our PMF estimations and, for comparison, the dynamical mass functions ($f(M)$) with the corresponding references. As expected, the latter two are fully consistent within the uncertainties.

The similarity of the optical and NIR correlations implies that the widths of Hα and the NIR lines, during quiescence, are consistent. This result was expected, since both Hα and the NIR emission lines are tracing the velocity from similar outer regions of the disc (~40% R_{L1}; see Sect. 3). The profiles of spectral disc emission lines from SXTs during outburst have shown both similarities (e.g., between Hα and He I λ10830) and differences (e.g., between Brγ with He I λ10830; Sánchez-Sierras & Muñoz-Darias 2020) that might be caused by the presence of outflows. In quiescence, however, given the lack of strong accretion activity, we expect the hydrogen and helium transitions to remain mostly unaltered. In the cases were we could measure the width of more than one emission line, we observe that the values are consistent within errors. In order to analyse the correlation for these transitions separately, additional simultaneous data are required.

Using a sample of cataclysmic variables, Casares (2015) showed that the slope of the FWHM–K_2 correlation decreases with increasing mass ratio q. We note that one of our systems, Aql X-1, is a NS SXT with $q = 0.41 \pm 0.08$ (Mata Sánchez et al. 2017), while the others are BH SXTs with typical mass ratios $q \sim 0.1$. This may explain why Aql X-1 lies slightly under the correlation in Fig. 2. However, a single data point is not enough to make strong assumptions, and more observations of NS SXTs are needed for confirmation.

Following with exploiting relations to derive fundamental parameters from faint SXTs, future work should employ NIR emission lines to explore the correlations previously established using Hα. In particular, Casares (2016) reported a correlation between the mass ratio (q) and the ratio of the double-peaked separation to the FWHM of Hα. Subsequently, a correlation between the binary inclination and the depth of the trough from the double-peaked Hα was presented by Casares et al. (2022).

5. Conclusions

In this work, we compiled quiescent NIR spectra of SXTs – mainly BHs – with known K_2 values, and measured the FWHM of He I λ10830, Paγ and/or Brγ emission lines. We present a NIR FWHM–K_2 correlation that allow us to estimate K_2 of faint SXTs from single-epoch spectroscopy, saving substantial observing time when compared to the phase-resolved radial velocity method. We find that this NIR correlation is fully consistent with its optical analogue. This result, together with the similarity of the FWHM values of different NIR lines in a given system, suggests that any H or He I transition could be useful for estimating K_2. Most importantly, we are then able to constrain the mass function of the compact object in the system by combining the FWHM–K_2 relation with $P_{\rm orb}$. This new NIR correlation will not only reveal the nature of highly-reddened SXTs, but will also expand the Galactic BH statistics, allowing for detailed studies of their formation mechanisms.

Acknowledgements. We thank the anonymous referee for their useful and thoughtful comments, which helped to improve this Letter. This work is supported by the Spanish Ministry of Science via the Plan de Generacion de conocimiento: PID2020-120323GB-I00 and PID2021-124879NB-I00, and an Europa Excelencia grant (EUR2021-122010). We acknowledge support from the Consejería de Economía, Conocimiento y Empleo del Gobierno de Canarias and the European Regional Development Fund (ERDF) under grant with reference ProID2021010132. We would like to thank D. Steeghs for providing the spectra of GRS 1915+105. We are also very grateful to Elizabeth J. Gonzalez for helpful discussions. This research has made use of the Keck Observatory Archive (KOA), which is operated by the W. M. Keck Observatory and the NASA Exoplanet Science Institute (NExScI), under contract with the National Aeronautics and Space Administration. We thank F. A. Cordova, PI of the A0620-00 dataset obtained through KOA. This research is based on observations (program ID GN-2011A-Q-13) obtained at the international Gemini Observatory, a program of NSF's NOIRLab, which is managed by the Association of Universities for Research in Astronomy (AURA) under a cooperative agreement with the National Science Foundation on behalf of the Gemini Observatory partnership: the National Science Foundation (United States), National Research Council (Canada), Agencia Nacional de Investigación y Desarrollo (Chile), Ministerio de Ciencia, Tecnología e Innovación (Argentina), Ministério da Ciência, Tecnologia, Inovações e Comunicações (Brazil), and Korea Astronomy and Space Science Institute (Republic of Korea). This research is also based on observations collected at the European Southern Observatory under ESO programme(s) 091.D-0921(A), 085.D-0497(A) and 085.D-0271(A), and data obtained from the ESO Science Archive Facility under programme(s) 097.D-0915(A) and 297.D-5048(A). MOLLY software (`http://deneb.astro.warwick.ac.uk/phsaap/software/molly/html/INDEX.html`) developed by Tom Marsh is gratefully acknowledged. We made use of `numpy` (Harris et al. 2020), `astropy` (Astropy Collaboration 2013, 2018), `scipy` (Virtanen et al. 2020) and `matplotlib` (Hunter 2007) PYTHON packages. We also used IRAF (Tody 1986) extensively.

References

Abbott, R., Abbott, T. D., Acernese, F., et al. 2023, Phys. Rev. X, 13, 011048
Astropy Collaboration (Robitaille, T. P., et al.) 2013, A&A, 558, A33
Astropy Collaboration (Price-Whelan, A. M., et al.) 2018, AJ, 156, 123
Belczynski, K., Wiktorowicz, G., Fryer, C. L., Holz, D. E., & Kalogera, V. 2012, ApJ, 757, 91
Casares, J. 2015, ApJ, 808, 80
Casares, J. 2016, ApJ, 822, 99
Casares, J. 2018, MNRAS, 473, 5195
Casares, J., & Jonker, P. G. 2014, Space Sci. Rev., 183, 223
Casares, J., Charles, P. A., & Naylor, T. 1992, Nature, 355, 614
Casares, J., Jonker, P. G., & Israelian, G. 2017, Handbook of Supernovae (New York: Springer International Publishing), 1499
Casares, J., Muñoz-Darias, T., Torres, M. A. P., et al. 2022, MNRAS, 516, 2023
Charles, P. A., & Coe, M. J. 2006, in Compact stellar X-ray sources, eds. W. Lewin, & M. van der Klis (Cambridge: Cambridge University Press), 215
Corral-Santana, J. M., Casares, J., Shahbaz, T., et al. 2011, MNRAS, 413, L15
Corral-Santana, J. M., Casares, J., Muñoz-Darias, T., et al. 2016, A&A, 587, A61
El-Badry, K., Rix, H. W., Cendes, Y., et al. 2023, MNRAS, 521, 4323
Fabian, A. C. 2012, ARA&A, 50, 455
Fender, R., & Muñoz-Darias, T. 2016, Lecture Notes in Physics (Berlin: Springer Verlag), 905, 65
Giesers, B., Dreizler, S., Husser, T. O., et al. 2018, MNRAS, 475, L15
González Hernández, J. I., & Casares, J. 2010, A&A, 516, A58
González Hernández, J. I., Rebolo, R., & Casares, J. 2012, ApJ, 744, L25
González Hernández, J. I., Suárez-Andrés, L., Rebolo, R., & Casares, J. 2017, MNRAS, 465, L15
Harris, C. R., Millman, K. J., van der Walt, S. J., et al. 2020, Nature, 585, 357
Harrison, T. E., Howell, S. B., Szkody, P., & Cordova, F. A. 2007, AJ, 133, 162
Heida, M., Jonker, P. G., Torres, M. A. P., & Chiavassa, A. 2017, ApJ, 846, 132

Hunter, J. D. 2007, Comput. Sci. Eng., 9, 90
Hynes, R. I., Zurita, C., Haswell, C. A., et al. 2002, MNRAS, 330, 1009
Jonker, P. G., Kaur, K., Stone, N., & Torres, M. A. P. 2021, ApJ, 921, 131
Kalogera, V., & Baym, G. 1996, ApJ, 470, L61
Khargharia, J., Froning, C. S., Robinson, E. L., & Gelino, D. M. 2013, AJ, 145, 21
Kiel, P. D., & Hurley, J. R. 2006, MNRAS, 369, 1152
Lam, C. Y., Lu, J. R., Udalski, A., et al. 2022, ApJ, 933, L23
Mata Sánchez, D., Muñoz-Darias, T., Casares, J., Corral-Santana, J. M., & Shahbaz, T. 2015, MNRAS, 454, 2199
Mata Sánchez, D., Muñoz-Darias, T., Casares, J., & Jiménez-Ibarra, F. 2017, MNRAS, 464, 41
McClintock, J. E., & Remillard, R. A. 2006, Compact Stellar X-ray Sources (Cambridge: Cambridge University Press), 157
Motta, S. E., Kajava, J. J., Giustini, M., et al. 2021, MNRAS, 503, 152
Reynolds, C. S. 2021, ARA&A, 59, 117
Rezzolla, L., Most, E. R., & Weih, L. R. 2018, ApJ, 852, L25
Romani, R. W. 1998, A Census of Low Mass Black Hole Binaries, Tech. rep.
Sahu, K. C., Anderson, J., Casertano, S., et al. 2022, ApJ, 933, 83
Sánchez-Sierras, J. & Muñoz-Darias, T. 2020, A&A, 640, L3
Smak, J. 1969, Acta Astron., 19, 155
Steeghs, D., Mcclintock, J. E., Parsons, S. G., et al. 2013, ApJ, 768, 185
Tetarenko, B. E., Sivakoff, G. R., Heinke, C. O., & Gladstone, J. C. 2016, ApJS, 222, 15
Tody, D. 1986, in Instrumentation in Astronomy VI, SPIE, 0627, 733
Torres, M. A. P., Casares, J., Jiménez-Ibarra, F., et al. 2019, ApJ, 882, L21
Virtanen, P., Gommers, R., Oliphant, T. E., et al. 2020, Nat. Methods, 17, 261
Wang, S., & Chen, X. 2019, ApJ, 877, 116
Wu, J., Orosz, J. A., McClintock, J. E., et al. 2015, ApJ, 806, 92
Yanes-Rizo, I. V., Torres, M. A. P., Casares, J., et al. 2022, MNRAS, 517, 1476
Yungelson, L. R., Lasota, J.-P., Nelemans, G., et al. 2006, A&A, 454, 559